J Mater Sci (2011) 46:1027–1037
DOI 10.1007/s10853-010-4868-7

FP-LAPW calculations of structural, electronic, and optical properties of alkali metal tellurides: M_2Te [M: Li, Na, K and Rb]

S. M. Alay-e-Abbas · A. Shaukat

Received: 30 May 2010 / Accepted: 23 August 2010 / Published online: 8 September 2010

Abstract Structural, electronic, and optical properties of alkali metal tellurides M_2Te [M: Li, Na, K, and Rb] are investigated in the framework of density functional theory within generalized gradient approximation. The calculated structural parameters are in excellent agreement with the experimental data. The electronic band structure calculations show that tellurides of Li, K, and Rb have an indirect fundamental energy band gap, whereas Na_2Te has a direct fundamental energy band gap. To explicate the contribution of anion and cation states to the electronic band structure, the electronic density of states for these compounds has been analyzed. Optical properties such as complex dielectric function, absorption coefficient, refractive index, extinction coefficient, and reflectivity are reported for a wide range of photon energy and are discussed on the basis of corresponding electronic band structure. Furthermore, the electron energy-loss functions for M_2Te compounds are also predicted. In order to validate the performance of the ab initio calculation reported herein, we systematically study the electronic and optical properties of wide band gap M_2Te compounds and compare them with available theoretical and experimental data of M_2O, M_2S, and M_2Se compounds.

Introduction

Alkali metal tellurides M_2Te [M: Li, Na, K, and Rb], as promising photo-emissive ultraviolet light materials, have undergone extensive research activities due to their excellent photocathodic quantum efficiencies, low energy dispersion of photoelectrons, and short response to pulsed light [1–3]. Their novel superionic conductivity has also attracted technological interest of a number of researchers [4–7]. Most of the theoretical studies for alkali metal tellurides have been dedicated to their structural properties such as lattice constants and bulk modulus [8–12] or to the phase diagrams of these materials [13–16]. Electronic band structures of some M_2Te compounds have been recently predicted by Eithiraj et al. [17] and Seifert-Lorenz and Hafner [18] using tight-binding linear muffin-tin orbitals (TB-LMTO) method and pseudopotentials method, respectively, in the frame work of density functional theory (DFT). From experimental point of view, absorption spectra [19] at high temperatures and thermodynamic properties of solutions of alkali metal tellurides in the melt LiCl and LiCl–LiF [20] are also available in literature; however, no experimental study has been performed for electronic and optical properties of these materials at ambient temperature and pressure.

Despite the fact that many alkali metal chalcogenides were synthesized and identified as face-centered cubic crystals many years ago [21], there are still some gaps in our knowledge of the electronic band structure and optical properties of these compounds. Predicting intricate physical properties such as energy band-gaps and interband optical transitions using first-principles techniques without an experimental backing is a bold step. However, since the quantum mechanical description of the physical and physiochemical properties of alkali metal oxides [22] and sulfides [23] using sophisticated many-body techniques have been found to agree well with experimental data and also because these compounds form a homologous series of crystalline solids with predictable electronic and optical properties, in our recent study [24] we have been able to

S. M. Alay-e-Abbas
Department of Physics, GC University, Allama Iqbal Road, Faisalabad 38000, Pakistan

A. Shaukat (✉)
Department of Physics, University of Sargodha, Sargodha 40100, Pakistan
e-mail: schaukat@gmail.com

close one such gap for alkali metal selenides using the full-potential linearized augmented plane-wave (FP-LAPW) method in the framework of DFT.

In this study, we present a series of first-principle DFT calculations on the electronic and optical properties of dialkali monotellurides. We have investigated the frequency-dependent dielectric function, absorption coefficient, refractive index, extinction coefficient, and reflectivity of M_2Te compounds. Salient features and trends in the electronic band structures and optical properties of alkali metal tellurides have been analyzed in the light of available theoretical and experimental data of other group IA-VI crystals. This study may prove to be a milestone for future experimental investigations and a means to envisage technological applications of these materials.

Computational methods

The calculations have been performed using the full-potential linearized augmented plane-wave (FP-LAPW) method in the framework of density functional theory as implemented in the WIEN2K code [25]. The exchange and correlation effects have been treated within generalized gradient approximation (GGA) functional proposed by Wu and Cohen (WC-GGA) [26] for structural and electronic properties, whereas the GGA parameterization scheme proposed by Engel and Vosko (EV-GGA) [27] has been used for electronic and optical properties calculations only. A muffin-tin model for the crystal potential is assumed in these calculations for partitioning the core and valence electrons. Linear combination of radial solution of the Kohn–Sham equation times the spherical harmonic has been utilized inside the non-overlapping muffin-tin spheres. In the interstitial region plane-wave basis sets have been utilized and plane-wave cut-off value of $K_{\max} \times R_{\mathrm{MT}} = 9$ has been used to control the size of basis set for wave functions. The R_{MT} values for Li, Na, K, Rb, and Te have been taken to be 1.6, 2.1, 2.3, 2.5, and 2.7 a.u, respectively, after performing several tests for energy convergence. The maximum value of angular momentum, $l_{\max}$ for the wave function expansion inside the atomic spheres has been taken at 10 and a mesh of 72 k-points has been used for the Brillion zone integrations in the corresponding irreducible wedge.

To compute the possible direct and indirect interband optical transitions in a solid-state material, one needs to calculate the tensor components of the complex dielectric function $\varepsilon(\omega)$. Due to the cubic symmetry of the crystal structure of the compounds under study, alkali metal tellurides can be treated as isotropic in relation to propagation of light. Therefore we need to compute only one component of the dielectric tensor. The imaginary part ($\varepsilon_2(\omega)$) of the incident photon's frequency (ω) dependent complex dielectric function is given by [28]:

$$\varepsilon_2(\omega) = \frac{e^2\hbar}{\pi m^2\omega^2}\sum_{v,c}\int_{BZ}\left[|M_{cv}(k)|^2\delta[\omega_{cv}(k)-\omega]\right]\mathrm{d}^3k \quad (1)$$

where the integral is over the first Brillouin Zone (BZ), $M_{cv}(k) = \langle u_{ck}|\delta\cdot\nabla|u_{vk}\rangle$ are the momentum dipole elements and δ is the potential vector defining electric field. $M_{cv}(k)$ are the matrix elements for direct transitions between valence band states $|u_{vk}\rangle$ and conduction band states $\langle u_{ck}|$. The corresponding transition energy for these states is $\hbar\omega_{cv} = E_{ck} - E_{vk}$. The real part of the dielectric function can be obtained from the imaginary part using the Kramers–Krönig relation [29],

$$\varepsilon_1(\omega) = 1 + \frac{2}{\pi}P\int_0^\infty \frac{\omega'\varepsilon_2(\omega')}{\omega'^2-\omega^2}\mathrm{d}\omega' \quad (2)$$

where, P is principle value of the integral. In order to accurately compute $\varepsilon_1(\omega)$ and to ensure convergence, we have calculated $\varepsilon_2(\omega)$ up to 65 eV and have used this value as truncation energy in Kramers–Krönig relation. The calculations for real and imaginary parts of the dielectric function have been performed using a dense mesh of k-points within the EV-GGA.

From the knowledge of the real and imaginary parts of the dielectric function, various optical parameters can be calculated. We have computed the reflectivity from the Fresnel's formula:

$$R(\omega) = \left|\frac{\sqrt{\varepsilon(\omega)}-1}{\sqrt{\varepsilon(\omega)}+1}\right|^2 \quad (3)$$

The absorption coefficient $I(\omega)$ and the energy-loss function $L(\omega)$ have been explicitly calculated using,

$$I(\omega) = 2\omega\left(\frac{[\varepsilon_1^2(\omega)+\varepsilon_2^2(\omega)]^{1/2}-\varepsilon_1(\omega)}{2}\right)^{1/2} \quad (4)$$

$$L(\omega) = \frac{\varepsilon_2(\omega)}{\varepsilon_1^2(\omega)+\varepsilon_2^2(\omega)} \quad (5)$$

and the extinction coefficient k and the refractive index n from the expressions:

$$k(\omega) = \left[\frac{[\varepsilon_1^2+\varepsilon_2^2]^{1/2}-\varepsilon_1}{2}\right]^{1/2} \quad (6)$$

$$n(\omega) = \left[\frac{[\varepsilon_1^2+\varepsilon_2^2]^{1/2}+\varepsilon_1}{2}\right]^{1/2} \quad (7)$$

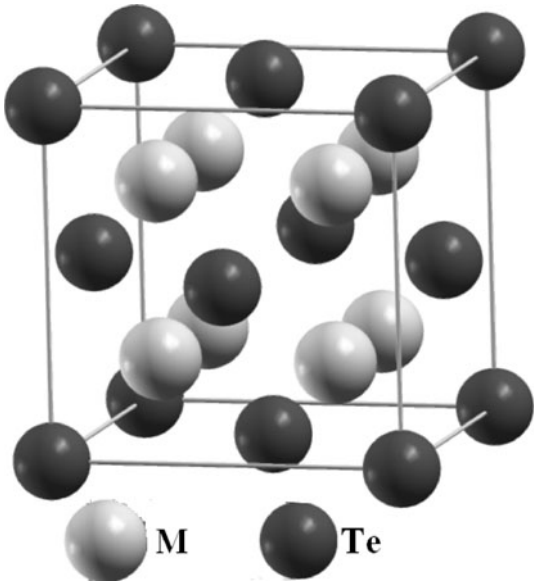

Fig. 1 Atomic structure of the anti-CaF_2-type M_2Te showing the face-centered cubic packing of (Te) anions, with (M) cations located in all the Te tetrahedral

Results and discussions

Structural parameters

In this study, the compounds under investigation have been modeled in the anti-CaF_2-type crystal structure. Three members of this crystal family (Li_2Te, Na_2Te, and K_2Te) crystallize stably into the anti-CaF_2 (anti-fluorite)-type crystal structure ($F_m\bar{3}_m$, space group No. 225) at room temperature [21] except for dirubidium telluride, which is metastable in anti-fluorite-type structure and transforms irreversibly into anti-cotunnite (anti-$PbCl_2$)-type structure upon warming [30, 31]. The calcium fluoride (CaF_2) crystal is one of the most common ordered crystals type found in nature and is often termed as *fluorite*-type structure. CaF_2 has a basic structure that can be described as face-centered cubic packing of cations, with anions in all of the tetrahedral holes. Contrary to the CaF_2 structure, the anti-CaF_2 structure has a basic face-centered cubic packing of anions, with cations at the tetrahedral holes. In the M_2Te [M: Li, Na, K, and Rb] compounds, the metal atoms (M) are located at (0.25; 0.25; 0.25) and (0.75; 0.75; 0.75) positions, whereas the tellurium atoms (Te) are located at (0; 0; 0) position as shown in Fig. 1. Only WC-GGA functional has been used to compute the equilibrium lattice constants (a_o), total energies (E_0), bulk modulus (B_0), and its pressure derivatives (B'), by fitting Murnaghan equation of state (EOS) [32] to the total energy versus volume curves of these materials. The calculated structural parameters have been listed in Table 1 along with available theoretical and experimental data. A closer look at Table 1 shows that our results are in better agreement with experimental values compared with previous calculations, because of the use of accurate FP-LAPW method. As observed in the case of

Table 1 Lattice parameters a_o (Å), total energy E_0 (Ry), bulk modulus B_0 (GPa), and its pressure derivative B' for alkali metal tellurides

	Present study WC GGA	Experimental	TB-LMTO[b]	Other theoretical studies
Li_2Te				
a_0	6.478	6.517[a]	6.559	–
E_0	−13622.45175		−13609.6931	–
B_0	26.8394		26.18	51[c], 30.5[d], 29.6[e]
B'	4.6489		–	–
Na_2Te				
a_0	7.285	7.314[a]	7.246	–
E_0	−14241.51768		−14227.454	–
B_0	19.7235		21.47	32[c], 19.7[d], 23.9[e]
B'	4.7739		–	–
K_2Te				
a_0	8.114	8.220[a]	8.152	8.233[f]
E_0	−15999.756070		−15983:5524	–
B_0	13.7849		13.99	21[c], 15.1[d], 19.6[e], 12.9[f]
B'	4.9162		–	–
Rb_2Te				
a_0	8.460	8.490[g]	–	–
E_0	−25516.211524	–	–	–
B_0	12.0823	–	–	–
B'	4.8394	–	–	–

Results obtained in this study using WC-GGA along with available experimental and theoretical values

[a] Reference [21]

[b] Reference [17]

[c] Reference [10]

[d] Reference [9]

[e] Reference [11]

[f] Reference [18]

[g] Reference [31]

oxides [22], sulfides [23], and selenides [24] of alkali metals, the lattice constants and total energies of the system of alkali metal tellurides increase, whereas the bulk moduli decrease if one goes from $Li_2Te \rightarrow Rb_2Te$. The small values of bulk modulus show that these materials are highly compressible. Moreover, from the fact that the bulk modulus of these materials decreases from Li to Rb telluride it can be deduced that the compressibility of these materials is dependent on the radii of alkali metal atoms.

Electronic properties

In this section, we present the electronic properties of alkali metal tellurides in the anti-CaF_2 structure obtained using both WC-GGA and EV-GGA., while only the full relativistic band structures of EV-GGA along high-symmetry directions in BZ are shown in Fig. 2. It is well known that calculating band structures of solids is one of the many uses of the DFT, and the energy band gap is a critical property for understanding the electronic and optical properties of semiconductors in fabricating the semiconductor devices. This demands an accurate determination of the band gaps of these materials. In spite of the great success in performing remarkably well for a wide range of many-body problems in physics and chemistry, the standard local density approximation (LDA) and GGAs for the exchange-correlation functional in the Kohn–Sham formalism of the DFT are known to systematically underestimate the band gap of semiconductors by as much as ~50% due to self-interaction error [33–35]. This limitation in the calculations for semiconductors is a direct consequence of the assumption that quasiparticle energy band structure is similar to the band structure of noninteracting electrons that appears in the DFT. As a result of this assumption, the calculated band gap differs from the exact quasiparticle band gap by an amount of the so-called

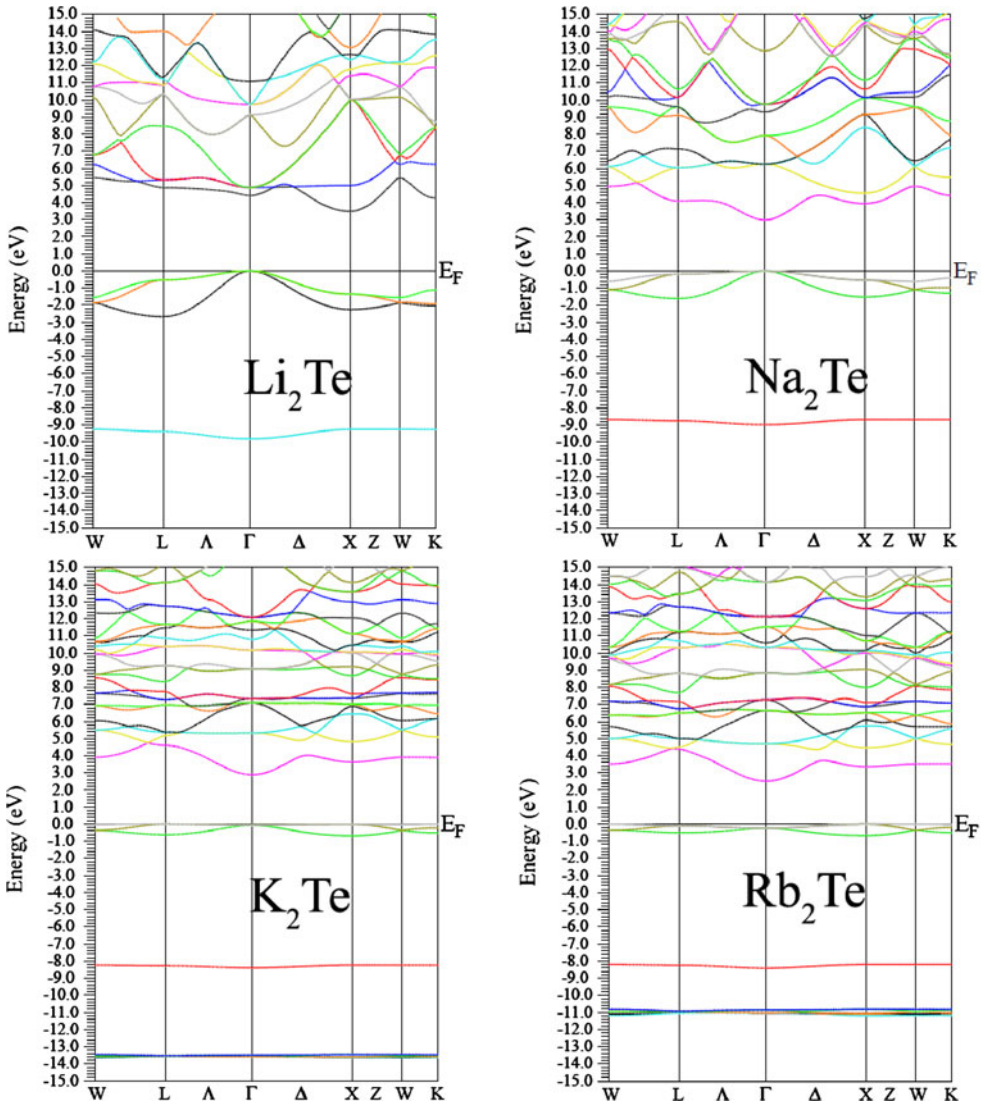

Fig. 2 Electronic band structure diagrams of Li_2Te, Na_2Te, K_2Te, and Rb_2Te compounds obtained with EV-GGA

"derivative discontinuity" (Δ) in the exchange-correlation potentials (V_{xc}) that should be taken into account explicitly for V_{xc} to restore the exact energy band gaps for semiconductors. Furthermore, due to the simple treatment of exchange-correlation energy in LDA parameterization schemes and GGA functionals other than the EV-GGA, the electronic, optical, and magnetic properties of semiconductors are either erroneously predicted [36] or too much overestimated [37]. On the other hand, unlike the simple GGA formalisms that are not able to reproduce both the exchange energy E_x and the exchange potential V_x, the EV-GGA is designed in such a way that it attempts to reproduce better V_x at the expense of less accurate exchange energy. This results in better band splitting and more accurate determination of some properties of semiconductors that are strongly dependent upon exchange-correlation potential [38, 39]. Nevertheless, constructing appropriate exchange-correlation functional which may be universally applicable remains an unresolved problem and a variety of approximation schemes including local-spin density (LSDA), GGA, meta-GGA, hyper-GGA, RPA+ have been discussed in the literature [40, 41].

Salient features of the electronic band structures presented in Fig. 2 can be analyzed in more detail on the basis of electronic density of states (DOS). For this reason we have calculated the total DOS, as well as partial DOS which are shown in Fig. 3a–d. A first look at Fig. 2 clearly shows that like the other chalcogenides of alkali metals, the tellurides of lithium, potassium, and rubidium have an indirect (X–Γ) band-gap, whereas Na_2Te has a direct band-gap. The Te s-like states contribute to the lowest band structures of Li_2Te, Na_2Te, K_2Te, and Rb_2Te appearing at −9.82, −9.01, −8.42, and −8.36 eV, respectively. K_2Te and Rb_2Te have additional low laying band structures due to cation p-like states at −13.52 and −11.04 eV, respectively. Most of the contribution to the valence bands of

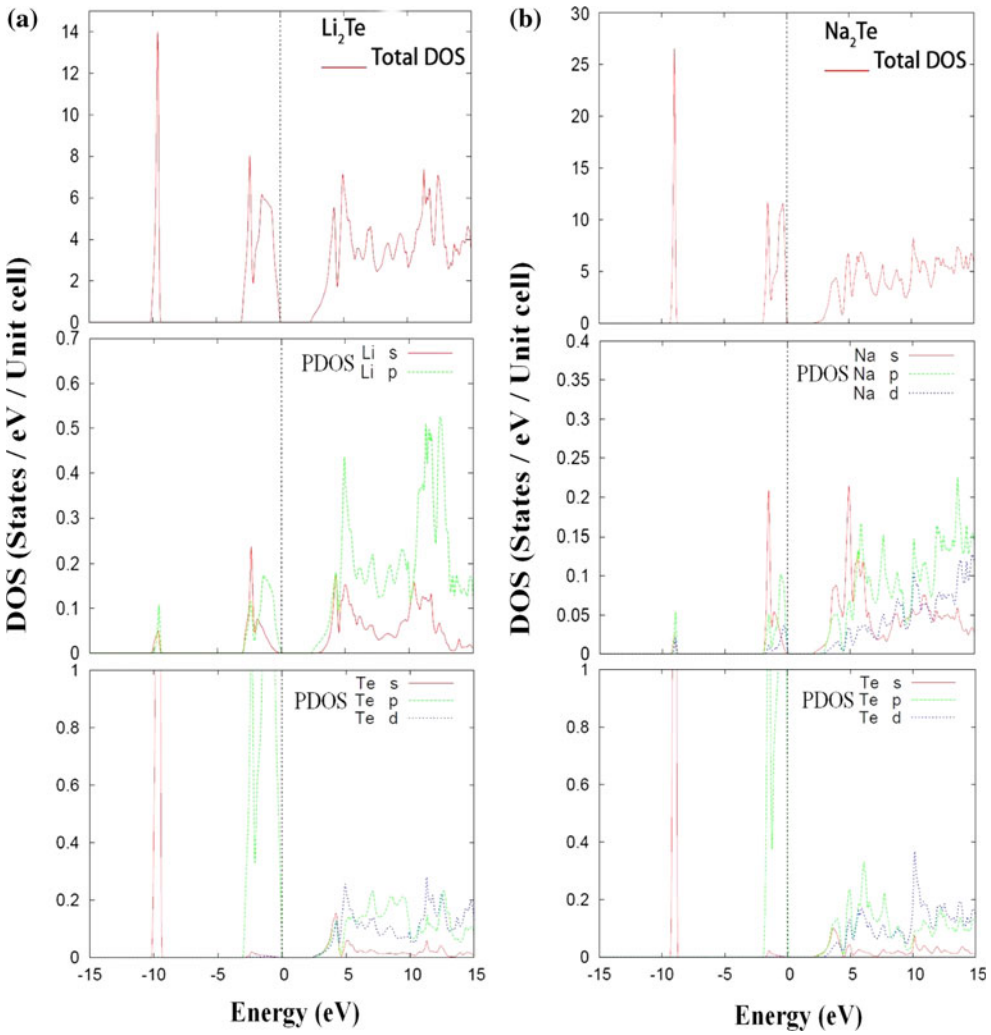

Fig. 3 Total and partial DOS for **a** Li_2Te, **b** Na_2Te, **c** K_2Te, and **d** Rb_2Te

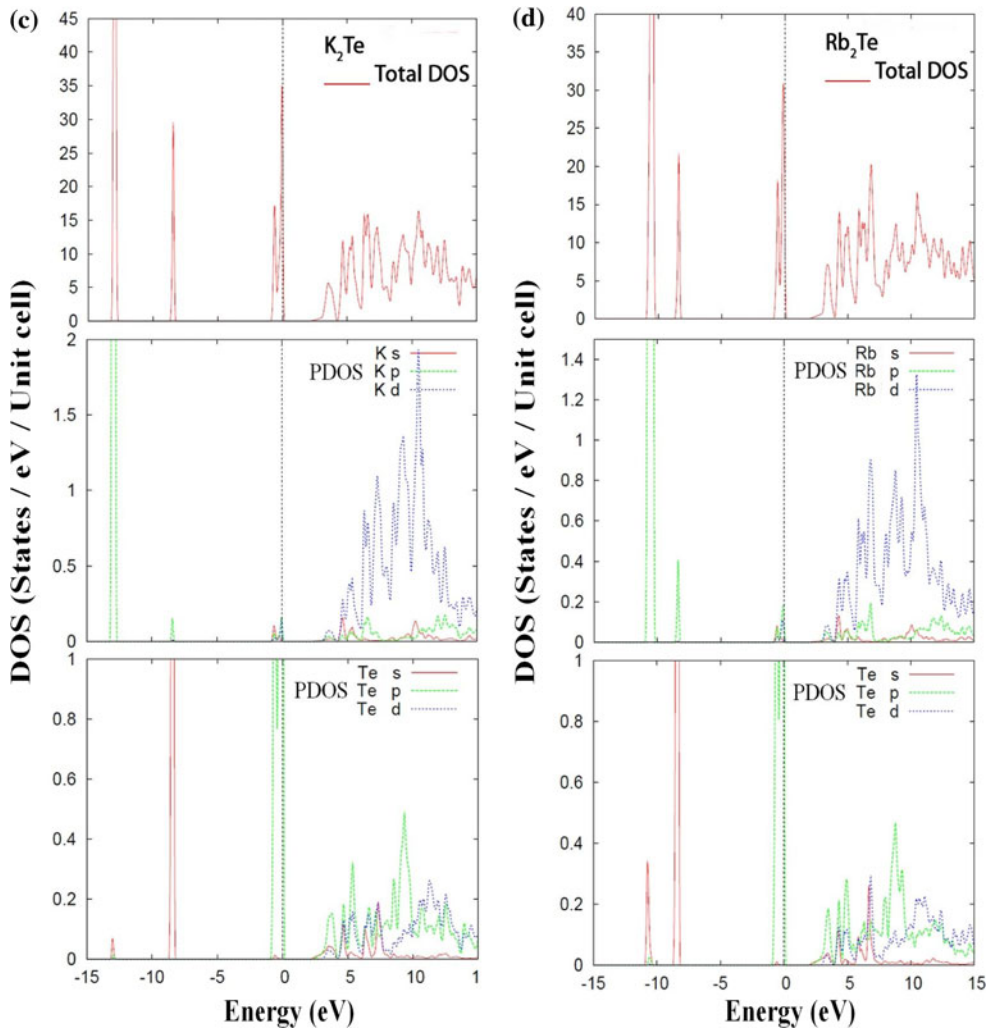

Fig. 3 continued

these materials comes from the anion *p* states with minor contributions from *s*- and *p*-like states of metal atoms. However, it is clear that the cation *s* like states contribute more to the lower portion of valence band and the cation *p* states contribute more to the upper portion (near Fermi level) of the valence band. The conduction band of these materials is made up of mixed contributions from *s*-, *p*- and *d*-like states of the M atoms and *p*- and *d*-like states of Te, however, for Li_2Te and Na_2Te the metal atom *p*-like states contribute more to the conduction band as compared to K_2Te and Rb_2Te for which the cation *d* states contribute more. Due to the hybridization caused by increasing size of the cation the band structure becomes more and more complex and the lowest energy band split into two bands as we go from lithium to rubidium telluride.

The calculated direct (Γ–Γ) and indirect (X–Γ) energy band gap values and the valence bandwidth of M_2Te compounds obtained with WC-GGA and EV-GGA are presented in Table 2 along with other available theoretical results obtained using the TB-LMTO [17] and pseudopotentials [18] methods. Since EV-GGA produces more accurate exchange-correlation potential as compared to WC-GGA, the values for energy gaps of the materials under study obtained with WC-GGA are lower in value than the ones obtained using EV-GGA. As observed in the FP-LAPW studies of oxides, sulfides, and selenides of alkali metals, the fundamental energy band gap of alkali metal tellurides decreases as one goes from Li to Rb due to the downward shift of the conduction band to the valence band as a consequence of increasing atomic number of cation. This decreasing trend in the fundamental energy band gap of these materials can be utilized for tailoring the band gaps of the mixed ternary alloys of alkali metal tellurides.

As already mentioned, no experimental data is available in literature for the electronic band structures of these materials. Therefore to validate the applicability of FP-LAPW calculations presented in this study we cite the

Table 2 Electronic band gap values and valence bandwidth calculated in this study using WC-GGA and EV-GGA for M_2Te compounds along with available theoretical results

Crystals	Energy band gap E_g (eV)		Valence bandwidth E_v (eV)
	Γ–Γ	X–Γ	
Li_2Te			
WC-GGA	3.07	2.39	2.43
EV-GGA	4.41	3.49	2.17
TB-LMTO[a]	3.289	2.258	1.711
Na_2Te			
WC-GGA	2.01	2.91	1.65
EV-GGA	2.96	3.49	1.42
TB-LMTO[a]	2.176	2.782	0.605
K_2Te			
WC-GGA	1.42	1.98	0.72
EV-GGA	2.88	2.81	0.65
TB-LMTO[a]	2.163	2.136	0.093
VASP[b]	2.166	2.160	0.65
Rb_2Te			
WC-GGA	2.17	1.95	0.76
EV-GGA	2.73	2.51	0.58
TB-LMTO[a]	–	–	–

[a] Reference [17]

[b] Reference [18]

theoretical study [23] in which the same method was utilized for alkali metal sulfides and it was observed that the valence bandwidth, Γ–Γ band gap and X–Γ band gap decrease with increasing size of cation. A similar behavior can be observed (See Table 2) in our FP-LAPW results for the aforementioned band structure parameters. Furthermore, the electron momentum spectroscopy results [42] of alkali metal oxides show that the inter-valence band gap at Γ-point of ionic crystals is dependent upon the overlap interactions between adjacent chalcogen atoms. As the interatomic interactions are proportional to the reciprocal of anion–anion distance squared $(1/d^2)$ [43], the band gap between the Te s and Te p states should be linearly dependent on $1/d^2$. In Fig. 4 we present the calculated Te s–Te p band gap and Te p valence bandwidth as a function of the reciprocal of nearest-neighbor Te–Te distance squared. As argued earlier, both parameters show a linear dependence on $1/d^2$.

Dielectric function and optical properties

The calculated real and imaginary parts of the complex dielectric function as a function of wide range of the incident photon's energy for the compounds under study are shown in Fig. 5. In Fig. 6, we present the calculated

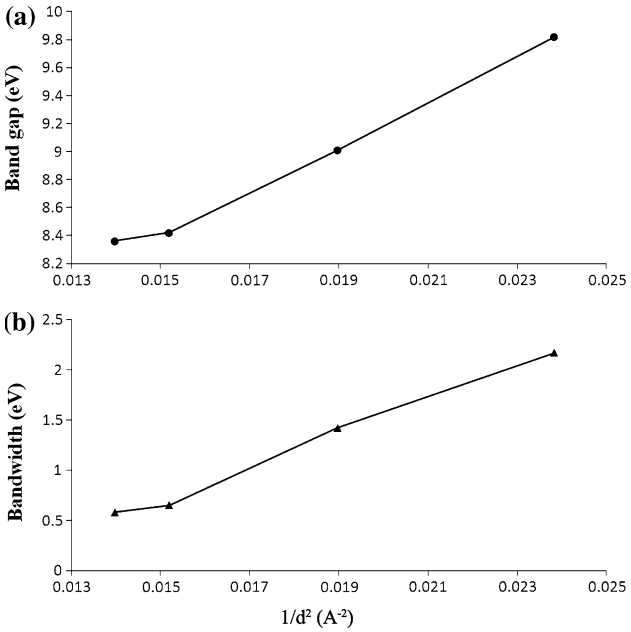

Fig. 4 **a** Calculated Te s–Te p band gap showing a linear dependence on $1/d^2$. **b** Calculated Te p valence bandwidth showing a linear dependence on $1/d^2$. d is the nearest-neighbor Te–Te distance

spectra of absorption coefficient (10^4 cm^{-1}), refractive index, extinction coefficient, and reflectivity of M_2Te semiconductors. The critical point structures in $\varepsilon_2(\omega)$, $k(\omega)$, and $I(\omega)$ for Li_2Te, Na_2Te, K_2Te, and Rb_2STe are listed in Table 3. It can be readily seen that the spectra of $\varepsilon_2(\omega)$ varies greatly for these materials which can be attributed to the fact that overall profiles of the conduction bands of these compounds are quite different. Since $\varepsilon_2(\omega)$ is closely connected with the energy band structure, the threshold for $\varepsilon_2(\omega)$ in the case of Li_2Te appearing at 5.56 eV is due to the direct optical transitions between the highest valence band and lowest conduction band along the L and X direction. The small bent about 7 eV is related to direct optical transition along the W and Δ edges. For Na_2Te the first peak, which is the main peak, located at 4.83 eV corresponds to direct transitions about the X-direction. The second peak appearing at 6.01 eV is due to direct Δ–Δ transitions, whereas, the small bent appearing at 6.22 eV corresponds to W–W transitions. The peaks for K_2Te located at 4.31, 5.10 (main peak), and 6.84 eV and for Rb_2Te located at 3.98, 4.77 (main peak), and 7.06 eV, originate from direct transitions along Λ, W, and L, respectively.

From the knowledge of the real part of the dielectric function, $\varepsilon_1(\omega)$, we can determine an important physical quantity, namely, the static dielectric constant $\varepsilon_1(0)$, which is defined as the low energy limit of real part of dielectric function and represents the dielectric response of a material to a static electric field. Listed in Table 3 are the static

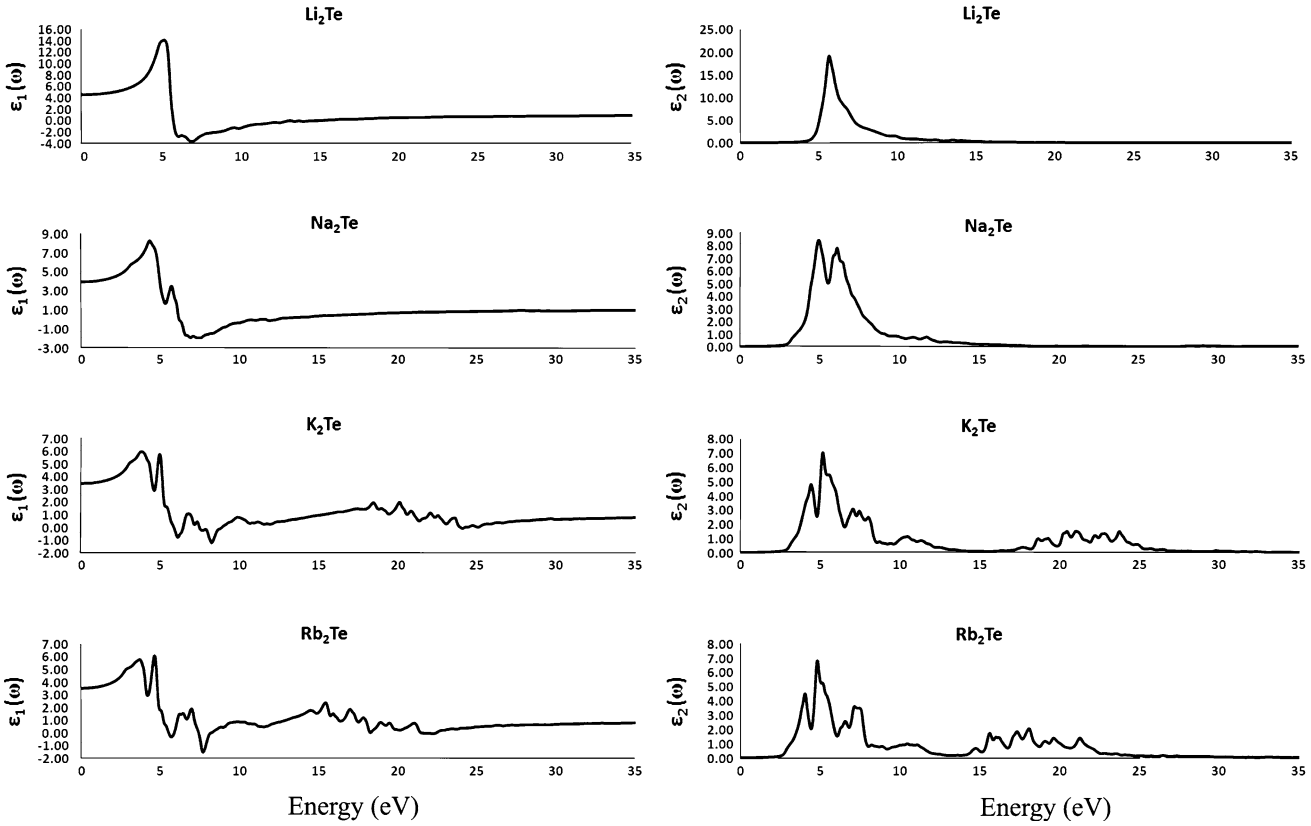

Fig. 5 The real part $\varepsilon_1(\omega)$ (*left panel*) and imaginary part $\varepsilon_2(\omega)$ (*right panel*) of the incident photon's energy complex dielectric functions for alkali metal telluride crystals

dielectric constants of Li_2Te, Na_2Te, K_2Te, and Rb_2Te along with the screened plasma frequencies ω_p of the same which are defined as the zero crossing of real part of dielectric function. The regions of incident photon energy where $\varepsilon_1(\omega) > 0$, electromagnetic radiation can propagate through a material and where $\varepsilon_1(\omega) < 0$, photons are damped and for $\varepsilon_1(\omega) = 0$, only longitudinally polarized waves are possible.

A comparison of $I(\omega)$ given in Fig. 6 with the spectra of imaginary part of dielectric function reveals that strong absorption regions for these materials occur where $\varepsilon_2(\omega)$ has large values. These absorption regions are the incident photon energy ranges in which these materials should be optically excited. For the absorption coefficient calculations, eigen-absorption was taken into account since $I(\omega)$ is not influenced by the polarized absorption [44]. The sharp edges of absorption coefficient and extinction coefficient given in Table 3 also show close relationship with $\varepsilon_2(\omega)$. These sharp edges in k and I for semiconductors emerge due to the fact that incident photons having energy less than the required energy to raise an electron across a band gap are unable to cause optical excitation. The absorption regions for M_2Te compounds occurring between 4 and 9 eV suggest that these materials may find applications in ultraviolet (UV) opto-electronic devices. Furthermore, in case of K_2Te and Rb_2Te large values of absorption coefficient also occur around 20 eV showing that these materials can find applications in opto-electronic devices requiring absorption of extreme-UV radiations. The variation of refractive index shown in Fig. 6 closely follows $\varepsilon_1(\omega)$, whereas, extinction coefficient changes as $\varepsilon_2(\omega)$. Furthermore, the variation of the extinction coefficient spectra of alkali metal tellurides show that the attenuation capabilities of these materials for UV radiations decreases in the fashion $Li_2Te \rightarrow Na_2Te \rightarrow K_2Te \rightarrow Rb_2Te$. The reflectivity for all these materials starts around 10%. Maximum values of reflectivity for Li_2Te, Na_2Te, K_2Te, and Rb_2Te are 48.77, 35.58, 30.16, and 29.20% at 5.56, 6.05, 5.07, and 4.74 eV, respectively. For the tellurides of lithium and sodium the reflectivity spectra decreases up to 10.05 and 8.72 eV, respectively, followed by smaller peaks around 16 eV after which the reflectivity becomes zero. In case of K_2Te and Rb_2Te, the reflectivity falls off to zero at 14.78 and 12.74 eV, respectively. Beyond this energy range, the reflectivity of K_2Te and Rb_2Te again shows higher values around 22 eV.

The energy-loss spectra shown in Fig. 7 for M_2Te compounds under study show the peaks at different energy

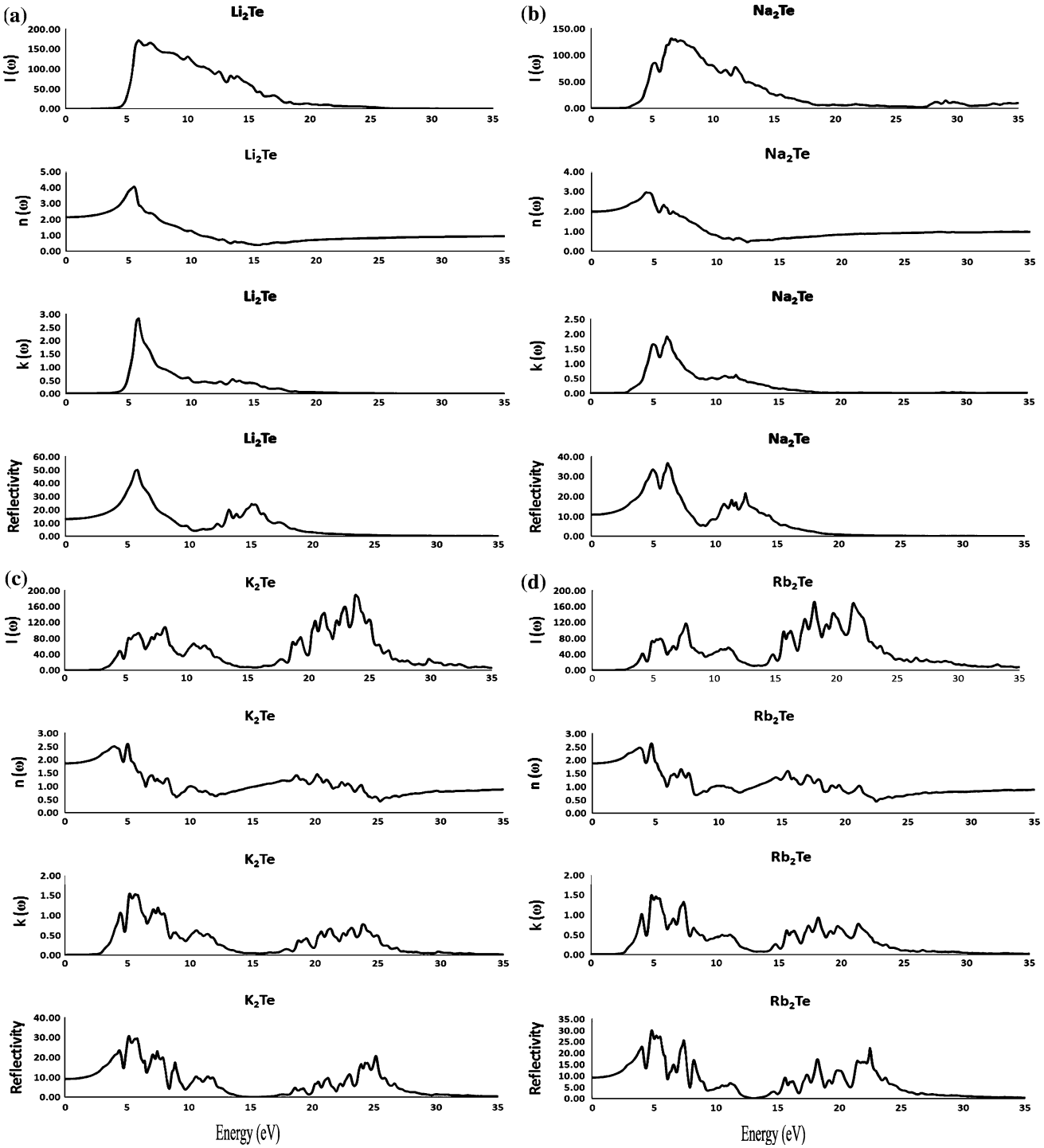

Fig. 6 The calculated absorption coefficient $I(\omega)$, refractive index $n(\omega)$, extinction coefficient $k(\omega)$, and reflectivity of **a** Li_2Te, **b** Na_2Te, **c** K_2Te, and **d** Rb_2Te crystals as a function of incident photon energy ($\hbar\omega$)

ranges corresponding to electronic excitations of different orbitals. The electron energy-loss function describes the possible interactions of an electron inside a solid, which are responsible for phonon excitation, interband and intraband transitions, plasmon excitations, inner shell ionizations, and Čerenkov radiations. Energy-loss spectra have broad bands between 8 and 18 eV for Li_2Te and Na_2Te, whereas for K_2Te and Rb_2Te, the broad bands in energy-loss function appear between 16 and 26 eV. The global maxima of energy-loss function (Fig. 7) occurs at 15.38, 12.42, 25.21, and 22.48 eV for tellurides of Li, Na, K, and Rb, respectively. These global maxima fit very well with the

Table 3 Calculated optical parameters for alkali metal tellurides

Crystals	Static dielectric constant $\varepsilon_1(0)$	Plasma frequencies ω_p (10^{16} rad/s)	Critical point values		
			ε_2	I	k
Li_2Te	4.55	2.27	4.09	4.06	3.88
Na_2Te	3.94	1.89	2.73	2.81	2.62
K_2Te	3.47	3.69	2.63	2.78	2.57
Rb_2Te	3.51	3.40	2.21	2.47	2.16

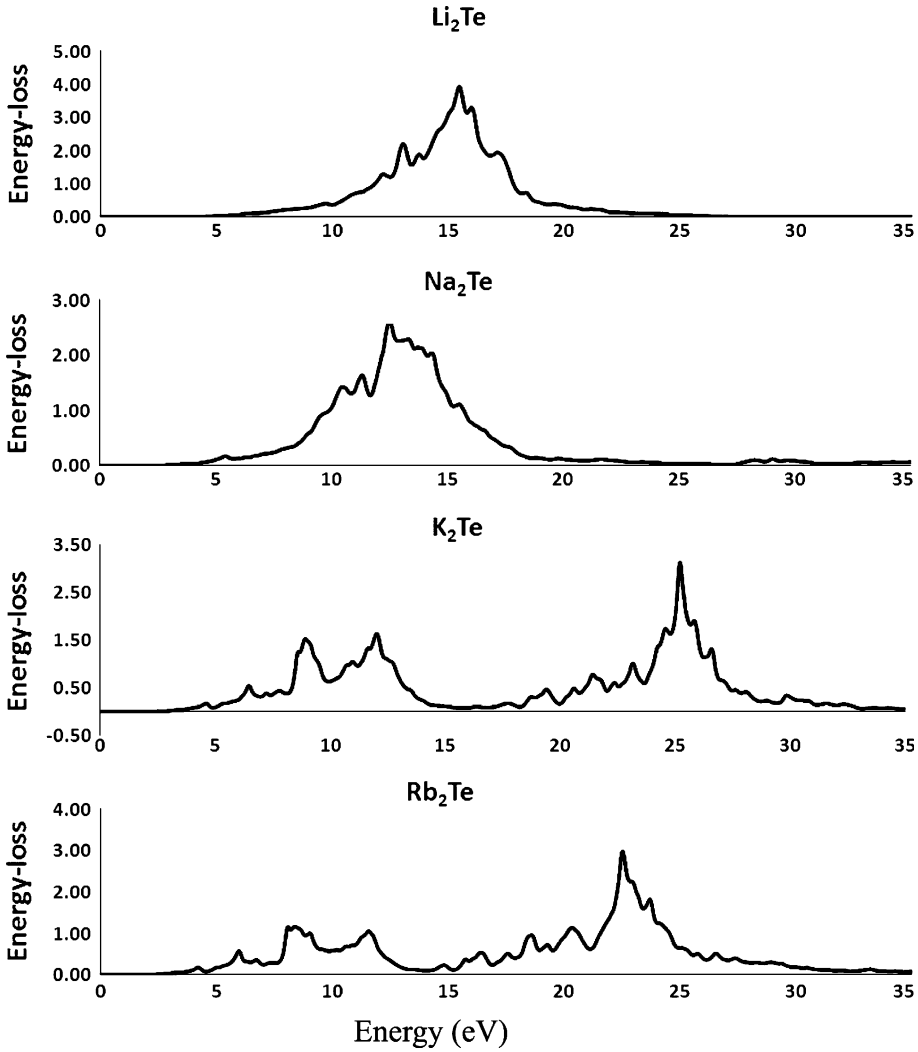

Fig. 7 Electron energy-loss function calculated using FP-LAPW method for alkali metal tellurides

rapid decrease in reflectivity shown in Fig. 6 and correspond to the electronic transitions from occupied M and Te atoms *p* and *d* states in the valence band to the Te *p* states of the conduction band. These maxima are larger than the other energy-loss peaks; because these are produced [45] as a result of rapid oscillations of the electron density in the form of a longitudinal wave with a characteristic plasma frequency (Table 3) in the volume of the crystal.

Conclusions

In summary, we have used FP-LAPW method based on density functional theory to investigate structural, electronic, and optical properties of alkali metal tellurides M_2Te [M: Li, Na, K, Rb] in anti-CaF_2 crystal structure. The generalized gradient approximation functional of Wu and Cohen has been utilized for structural properties, whereas

the GGA suggested by Engle and Vosko has been used in addition to the aforementioned GGA for electronic and optical properties calculations. Some trends in the electronic properties are discussed in the light of experimental and theoretical data of widely studied alkali metal oxides and sulfides. Our calculations show that Li_2Te, K_2Te, and Rb_2Te are indirect band gap materials and Na_2Te is a direct band gap material. The band-gap parameters obtained in this study are larger as compared to values reported in TB-LMTO and pseudopotential calculation. The structure of complex dielectric function has been analyzed to identify the possible optical interband transitions and is discussed based on the electronic band structure and DOS results of these materials. The Te *p* states and metal atom *p* and *d* states have been identified as initial and final states for the optical transitions in these compounds. Moreover, the refractive index, attenuation coefficient, reflectivity, and electron energy-loss function for alkali metal tellurides are presented along with theoretically calculated static dielectric constants and screened plasma frequencies.

References

1. Bisero D, di Bona A, Paradisi P, Valeri S (2000) J Appl Phys 87:543
2. Piccioli A, Pegna R, Fedorko I, Giunta M, Malakhov N, Menzione A, Raffaelli F, Braem A, Chesi E, Joram C, Séguinol J, Sartorl G, Weilhammer P (2004) Nucl Instr Meth Phys Res Sect A 518:602
3. Joram C (1999) Nucl Phys B (Proc. Suppl.) 78:407
4. Geller S (1997) Solid Electrolytes. Springer, Berlin
5. Vashishta P, Mundy JN, Shenoy GK (1979) Fast ion transport in solids. North-Holland, Amsterdam
6. Tuller HL, Balkanski M (1989) Science and technology of fast ion conductors. Plenum, New York
7. Kikuchi H, Iyetomi H, Hasegawa A (1989) J Phys Condens Matter 10:11439
8. Koh AK (1999) Phys Status Solidi (b) 210:31
9. Jain VK, Shanker J (1982) Phys Status Solidi (b) 114:287
10. Chaturvedi SD, Sharma SB, Paliwal P, Kumar M (1989) Phys Status Solidi (b) 156:171
11. Melillou A, Gupta BRK (1991) Czechoslov J Phys 41:813
12. Stöwe K (2004) Z Kristallogr 219:359
13. Sangster J, Pelton AD (1992) J Phase Equilib 3:303
14. Pelton AD, Petric A (1990) J Phase Equilib 11:447
15. Petric A, Pelton AD (1990) J Phase Equilib 11:443
16. Sangster J, Pelton AD (1997) J Phase Equilib 18:394
17. Eithiraj RD, Jaiganesh G, Kalpana G (2009) Int J Mod Phys B 23:5027
18. Seifert-Lorenz K, Hafner J (2002) Phys Rev B 66:094105
19. Gruen DM, McBeth RL, Foster MS, Crouthamel CE (1962) J Phys Chem 70:472
20. Foster MS, Liu CC (1966) J Phys Chem 7:950
21. Zintl E, Harder A, Dauth B (1934) Z Elektrochem 40:588
22. Moakafi M, Khenata R, Bouhemadou A, Khachai H, Amrani B, Rached D, Rérat M (2008) Eur Phys J B 64:35
23. Khachai H, Khenata R, Bouhemadou A, Haddou A, Reshak AH, Amrani B, Rached D, Soudini B (2009) J Phys Condens Matter 21:095404
24. Alay-e-Abbas SM, Sabir N, Saeed Y, Shaukat A (2010) J Alloys Compd 503:10
25. Blaha P, Schwarz K, Madsen GH, Kvasnicka D, Luitz J (2001) In: Schwarz K (ed) FP-L/APW + lo programe for calculating crystal properties, Technische Universität Wien, Vienna
26. Wu Z, Cohen RE (2006) Phys Rev B 73:235116
27. Engel E, Vosko SH (1993) Phys Rev B 47:13164
28. Ambrosch-Draxl C, Sofo JO (2006) Comput Phys Commun 175:1
29. Wooten F (1972) Optical properties of solids. Academic Press, New York
30. Sommer H, Hoppe R (1997) Z Anorg Allg Chem 429:118
31. Stöwe K, Appel S (2002) Angew Chem Int Ed Engl 41:2725
32. Murnaghan FD (1944) Prot Natl Acad Sci USA 30:244
33. Bachelet GB, Chrstensen NE (1985) Phys Rev B 31:879
34. Onida G, Reining L, Rubio A (2002) Rev Mod Phys 74:601
35. Fahy S, Chang KJ, Louis SG, Cohen ML (1989) Phys Rev B 35:7840
36. Terakura K, Oguchi T, Williams AR, Kübler J (1984) Phys Rev B 30:4734
37. Singh DJ, Askhenazi J (1992) Phys Rev B 46:11570
38. Dufek P, Blaha P, Schwarz K (1994) Phys Rev B 50:7279
39. Bouhemadou A, Khenata R, Zegrar F, Sahnoun M, Baltache H, Reshak AH (2006) Comput Mater Sci 38:263
40. Cohen AJ, Mori-Sanchez P, Yang W (2008) Phys Rev B 77:115123
41. Perdew JP, Schmidt K (2001) In: Van Doren VE, Van Alsenoy K, Greelings P (eds) Density functional theory and its applications to materials. American Institute of Physics. Melville
42. Mikajlo EA, Dorsett HE, Ford MJ (2004) J Chem Phys 120:10799
43. Harrison WA (1989) Electronic structure and the properties of solids. Dover, New York
44. Persson C, Ahuja R, Ferreira da Silva A, Johansson B (2001) J Cryst Growth 231:407
45. Xu M, Wang SY, Yin G, Li J, Zheng YX, Chen LY (2006) Appl Phys Lett 89:151908